SUPPLEMENTARY INFORMATION

Azobenzene Crystal Polymorphism Enables Tuneable Photoinduced Deformation, Mechanical Behaviors and Photoluminescent Properties

*Yunhui Hao, [a] Lei Gao, [a] Xiunan Zhang, [a] Rongli Wei, [a] Ting Wang, [a] Na Wang, [a] Xin Huang, *[a] Haifeng Yu *[b] and Hongxun Hao *[a]*

Table of Contents

1. Experimental Section

1.1 Materials

4-Aminobenzonitrile and bromoethane (Br-C_2H_5) were purchased from Aladdin Biochemical Technology Co., Ltd. Hydrochloric acid (HCl), sodium nitrite ($NaNO_2$), phenol, sodium acetate (CH_3COONa), ammonia water ($NH_3 \cdot H_2O$), potassium carbonate (K_2CO_3) and N, N-dimethylformide (DMF) were purchased from Tianjin Jiangtian Chemical Co., Ltd.

1.2 Equipment

^{1}H NMR spectra were recorded on a Bruker 500 MHz spectrometer to confirm the molecular structure of the synthesized compounds. All spectra were collected in chloroform-d ($CDCl_3$) solution. The light source for photoirradiation was a Height-LED HTLD-4 UV-LED light source (UV-light, 365 nm). Photoinduced deformation behaviors and force-induced mechanical behaviors were observed with a high-speed digital microscope (Stereo-microscope, Stemi 508, Carl Zeiss, Jena, Germany). The microscope images of photoluminescent were taken by Nikon E200. Thermal properties were determined by DSC analysis (Model name, Mettler Toledo, Co., Switzerland), with heating and cooling rates of 10 °C/min. Powder X-ray diffraction (PXRD) was performed on a Rigaku D/MAX 2500 with a scintillation counter. Single crystal X-ray diffraction data of Form I and Form II crystals were collected by Rigaku-Rapid II diffractometer. The crystal structures were solved by SHELXL and refined on F^2 by the full-matrix least-squares method. Atomic force microscopy (AFM) images were obtained by one scanning probe microscope in tapping mode (BioScope Resolve, Bruker Co., Ltd). Scanning electron microscopy (SEM) was performed on Hitachi TM3000. Nanoindentation tests were carried out on a Hysitron TI-Premier system. Dynamic mechanical analyses (DMA) were performed on a TA-DMA Q800 testing system. UV-vis absorption spectra of azobenzene in solution and UV-Vis diffuse reflection spectra of microcrystals were collected by a UV-3010 spectrophotometer (HITACHI, Japan). Raman spectra of straight crystals of two polymorphs and bent Form II crystal were recorded respectively using a micro-Raman spectrometer (inVia Reflex, Renishaw) with an excitation wavelength of 785 nm (diode laser) at a spectral resolution of 1 cm^{-1}. The photoluminescent (PL) spectra of crystals were measured using the same micro-Raman spectrometer with a 325 nm He-Cd laser. Absolute quantum efficiency was measured on an integrating sphere (FLS1000, Edinburgh Instruments).

2. Crystal growth and structural analysis of polymorphs

2.1 Syntheses

The azobenzene compound AzC_2 was synthesized according to our previously

reported method.[1] The chemical reaction is shown in Fig. S1, and the ^{1}H NMR spectra were recorded in CDCl$_3$ solution, as shown in Fig. S2.
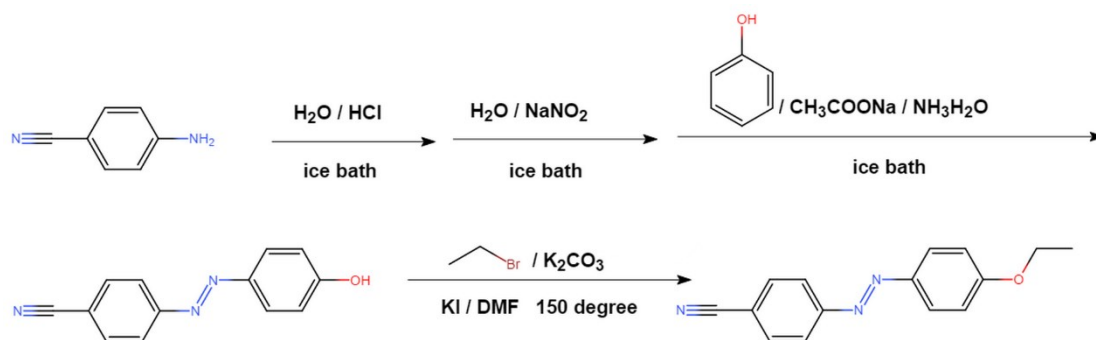

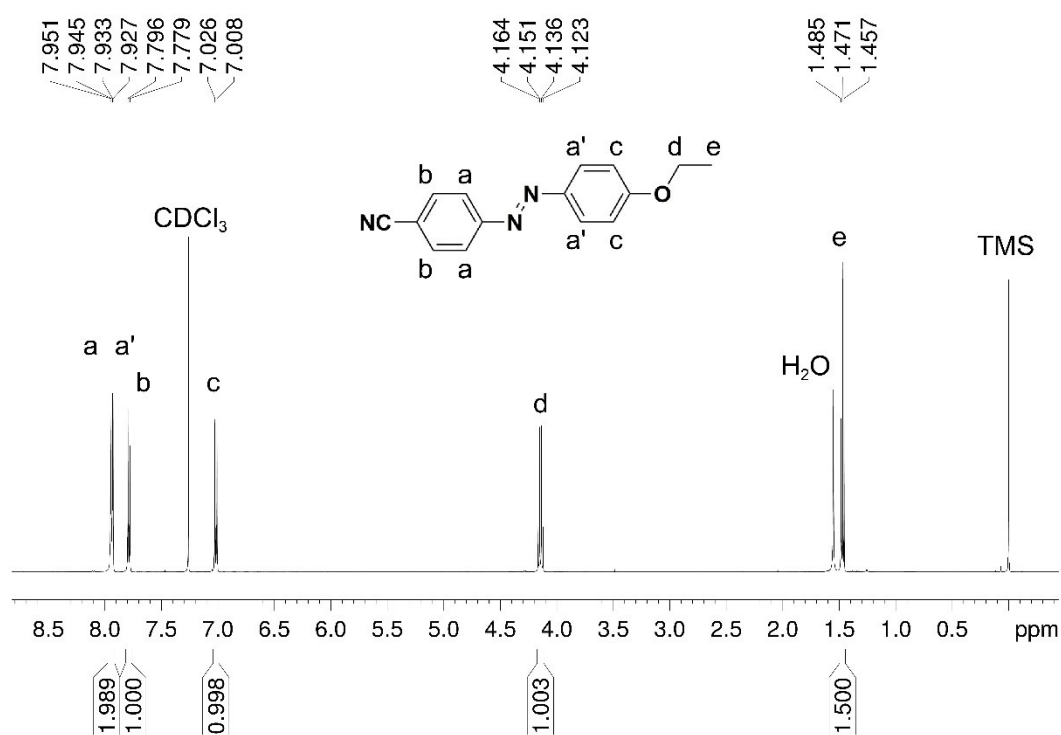**Fig. S1.** Synthesis of the photoactive azobenzene compound AzC$_2$.

Fig. S2. ^{1}H NMR spectra of the azobenzene compound AzC$_2$ (500MHz, CDCl$_3$, 25°C, TMS): δ 7.93-7.95 (4H, m), δ 7.78-7.80 (2H, d), δ 7.01-7.03 (2H, d), δ 4.12-4.16 (2H, d), δ 1.46-1.49 (2H, t). The peak at 1.53 ppm is due to water and the peak at 7.25 ppm is due to CDCl$_3$.

2.2 Preparation of microcrystals

The plate-like Form I microcrystals were prepared by sublimation method. The device is shown in Fig. S3a. Firstly, one quartz slide was fixed by adhesive tape at the bottom of the condensate tube as substrate, and 50 mg synthetic solid powder of AzC$_2$ was placed at the bottom of the sublimation crystallizer. Then, the breather bolt was

tightened, and the whole system was vacuumed by a pump. Meanwhile, the temperature of oil bath was kept at 90 °C for sublimation, and the temperature of circulating water bath was kept at 30 °C, 50 °C and 70 °C for condensation respectively. Finally, the plate-like microcrystals grew on the edges and surface of the quartz slide after several hours (Fig. S3b-d). With the increased condensation temperature, the crystal shape becomes more regular. Their PXRD patterns showed that they belonged to Form I (Fig. S3e-g).
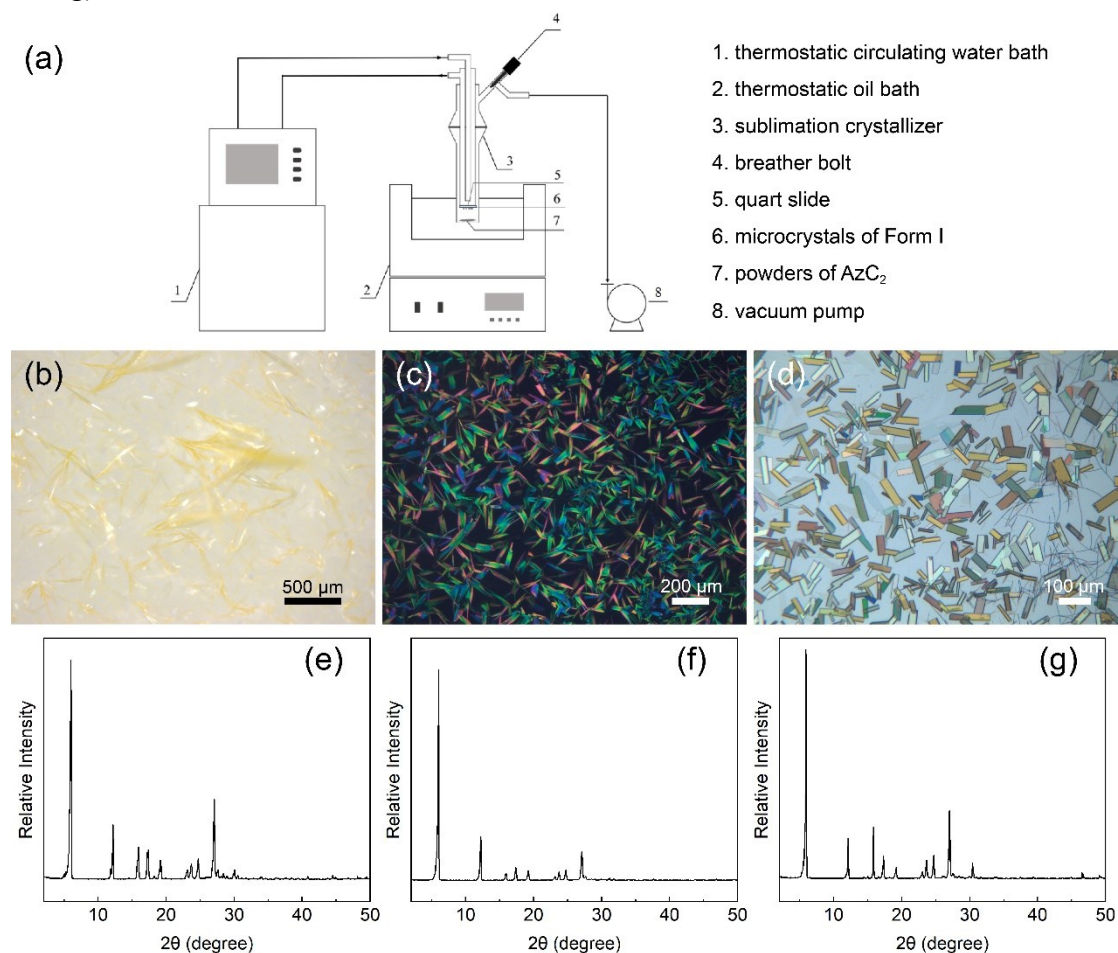
(a)

1. thermostatic circulating water bath
2. thermostatic oil bath
3. sublimation crystallizer
4. breather bolt
5. quart slide
6. microcrystals of Form I
7. powders of AzC_2
8. vacuum pump

(b)   500 µm

(c)   200 µm

(d)   100 µm

(e)

Relative Intensity

2θ (degree)

(f)

Relative Intensity

2θ (degree)

(g)

Relative Intensity

2θ (degree)

Fig. S3. (a) Schematic illustration of the sublimation crystallization device. (b-d) Microscope images of the plate-like microcrystals of Form I, which were obtained on the quartz slide by sublimation at 90 °C and condensation at (b) 30 °C, (c) 50 °C and (d) 70 °C respectively, and their corresponding PXRD patterns (e-g).

The needle-like Form II microcrystals were prepared through epitaxial crystallization. To start, 125 mg synthetic solid powder of AzC_2 and 10 mL methanol were added into 15 mL double-jacketed glass crystallizer and agitated by a magnetic stirrer at 400 rpm for about 30 min. The temperature was kept at 50 °C by a thermostat. When all the AzC_2 powders were completely dissolved, the stirring was stopped. Then, KBr (100) substrate was put into the crystallizer. The crystallizer was subjected to a relatively rapid cooling rate at 10 °C/h. Finally, the needle-like microcrystals with good shape grew at the interface between the KBr (100) substrate and the bottom of

crystallizer (Fig. S4a). The PXRD pattern showed that they belonged to Form II (Fig. S4b).
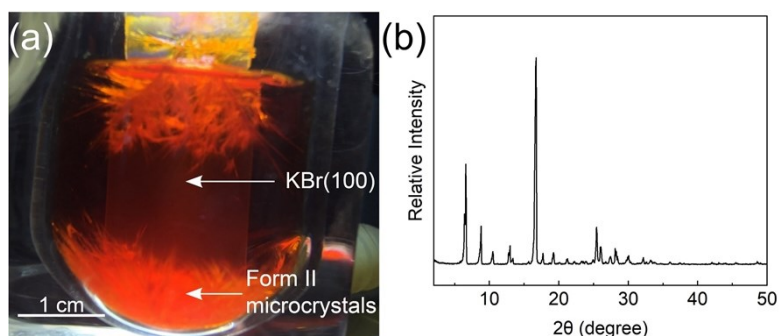

Fig. S4. (a) Photograph of the actual epitaxial crystallization of needle-like Form II microcrystals, and (b) the corresponding PXRD pattern.

2.3 Single Crystal X-ray Diffraction (SXRD)

To investigate the molecular packing in the two polymorphic crystal, large enough high-quality Form I and Form II single crystals of AzC_2 were further obtained. The Form I single crystal was cultivated by slow evaporation of the solvent of the ethyl acetate solution. The Form II single crystal was cultivated through epitaxial crystallization with a relatively slow cooling rate at 1 °C/h. Their PXRD shows good consistency with above microcrystals. Their X-ray crystallographic data are were presented in Table S1.
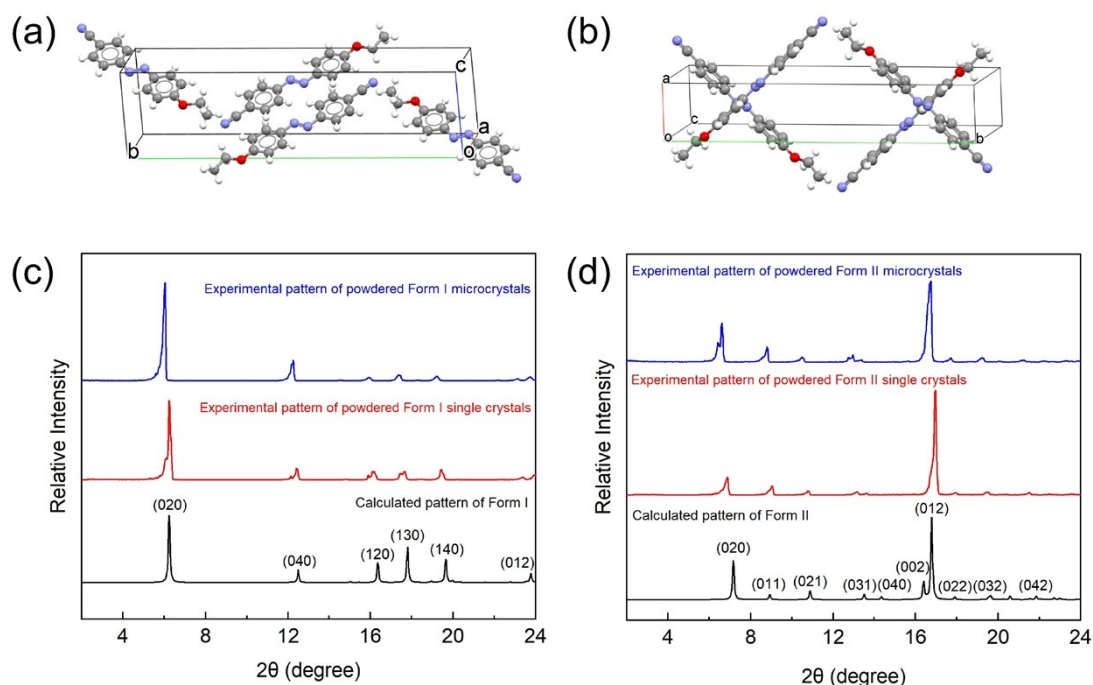

Fig. S5. Unit cells of (a) Form I and (b) Form II in stereo view. (c) PXRD patterns for Form I: calculated pattern of Form I (black line); experimental pattern of powdered Form I single crystals (red line); and experimental pattern of powdered Form I microcrystals (blue line). (d) PXRD patterns for Form II: calculated pattern of Form II

(black line); experimental pattern of powdered Form II single crystals (red line); and experimental pattern of powdered Form II microcrystals (blue line).
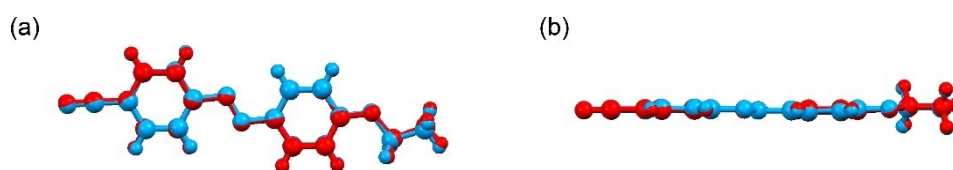

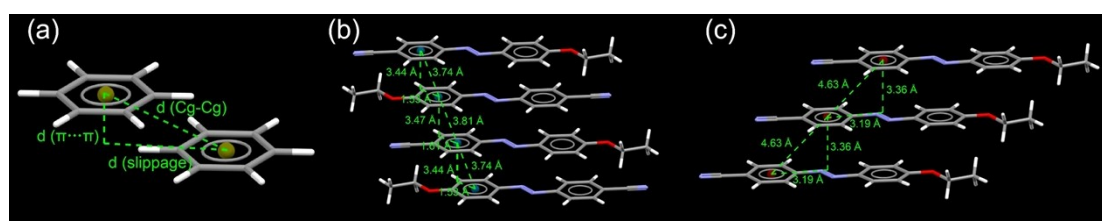**Fig. S6.** A head-on (a) and side-on (b) view of an overlay of Form I (blue) and Form II (red) of **trans-**AzC_2.

Fig. S7. (a) Schematic illustration of π-π stacking, where d (π···π) is the perpendicular distance of one aromatic ring centroid on another aromatic plain, d (Cg-Cg) is the distance between two aromatic ring centroids, and d (slippage) is the distance between the perpendicular projection of one aromatic ring centroid on another aromatic plain and the latter aromatic ring centroid. And schematic illustrations of π-π stackings in the crystal structures of (b) Form I and (c) Form II.

Table S1. X-ray crystallographic data of polymorph of **trans-**AzC_2.

Compounds	Form I		Form II	
CCDC No.	1944178		1944179	
Empirical formula	$C_{15}H_{13}N_3O$		$C_{15}H_{13}N_3O$	
Formula weight	251.28		251.28	
Color of crystal	orange-yellow		orange-red	
Temperature	113(2) K		113(2) K	
Wavelength	0.71073 Å		0.71073 Å	
Crystal system	Monoclinic		Monoclinic	
Space group	P2(1)/n		P2(1)/n	
Unit cell dimensions	a = 5.8621(11) Å	α = 90 °	a = 4.6333(11) Å	α = 90 °
	b = 28.318(5) Å	β = 91.238(4) °	b = 24.671(6) Å	β = 94.761(9) °
	c = 7.5488(15) Å	γ = 90°	c = 10.843(2) Å	γ = 90°

Volume	1252.8(4) Å^3	1235.1(5) Å^3
Z	4	4
Calculated density	1.332 Mg/m^3	1.351 Mg/m^3
Absorption coefficient	0.087 mm^{-1}	0.088 mm^{-1}
F (000)	528	528
Crystal size	0.20 x 0.18 x 0.12 mm^3	0.20 x 0.18 x 0.12 mm^3
Theta range for data collection	3.06 to 27.52°	3.11 to 27.54°
Limiting indices	-7<=h<=7, -36<=k<=36, -9<=l<=9	-5<=h<=5, -32<=k<=32, -13<=l<=14
Reflections collected / unique	15970 / 2886 [R(int) = 0.0265]	11951 / 2776 [R(int) = 0.0357]
Completeness to theta = 27.52°	99.7 %	98.2 %
Absorption correction	Semi-empirical from equivalents	Semi-empirical from equivalents
Max. and min. transmission	0.9897 and 0.9828	0.9895 and 0.9826
Refinement method	Full-matrix least-squares on F^2	Full-matrix least-squares on F^2
Data / restraints / parameters	2886 / 0 / 173	2776 / 0 / 173
Goodness-of-fit on F^2	1.073	1.022
Final R indices [I > 2sigma(I)]	R1 = 0.0384, wR2 = 0.1179	R1 = 0.0404, wR2 = 0.1194
R indices (all data)	R1 = 0.0448, wR2 = 0.1224	R1 = 0.0495, wR2 = 0.1245
Largest diff. peak and hole	0.379 and -0.186 e.Å^{-3}	0.355 and -0.155 e.Å^{-3}

2.4 Face indexing

The dominant surface of Form I and Form II microcrystals were indexed based on SEM observations, combining the results of preferred orientation from PXRD and the calculated Miller indices based on crystallographic data (Mercury).

One unground plate-like Form I microcrystal was placed in the holder so that the X-rays would mainly measure the large face. As shown in Fig. S8a, the sample showed two diffraction peaks (blue line). Compared these peaks with calculated XRD indexed patterns of Form I (black line), they represent the (020) and (040) surfaces. All of them are part of the same (00*l*) indices family, representing different parallel crystal planes. Hence, the dominant surface of plate-like Form I microcrystal observed by SEM was assigned to the (020) surface (Fig. S8b).
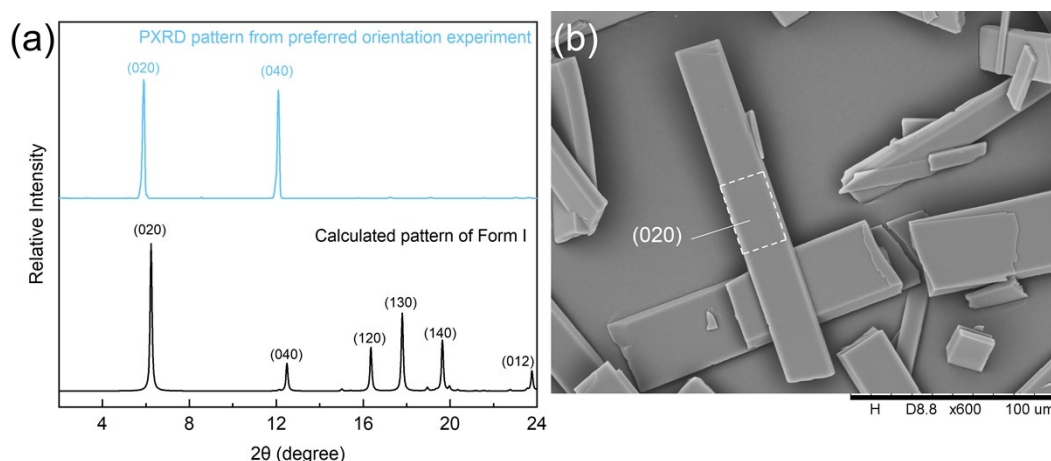
Fig. S8. (a) Calculated PXRD patterns of Form I (black line), and PXRD patterns from preferred orientation experiment of the dominant surface of Form I (blue line). (b) SEM picture of Form I and its face indexing.

On the other hand, the morphology of Form II microcrystal observed by SEM is cuboid (Fig. S9b), which means that it has two dominant surfaces. One unground needle-like Form II microcrystal was placed in the holder, and one of its dominant surfaces was facing upwards. As shown in Fig. S9a, only one diffraction peak was observed (red line). This peak represents plane (012) when compared with calculated XRD indexed patterns of Form II (black line). Then, the unground needle-like Form II microcrystal was rotated about 90 ° around its long axis, making another dominant surface facing upwards. By comparing its preferred orientation PXRD patterns (green line) with the calculated XRD indexed patterns of Form II (black line), this plane can be identified as the (020) face. Hence, the dominant surfaces of needle-like Form II microcrystal observed by SEM were assigned to the (012) and (020) surface.
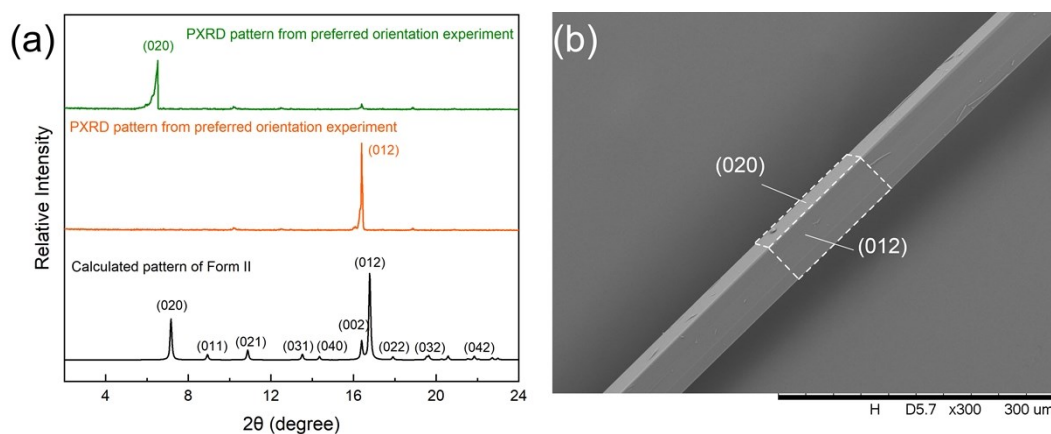

Fig. S9. (a) Calculated PXRD patterns of Form II (black line), PXRD patterns from preferred orientation experiment of one dominant surface of Form II (red line), and PXRD patterns from preferred orientation experiment of another dominant surface of Form II (green line). (b) SEM picture of Form II and its face indexing.
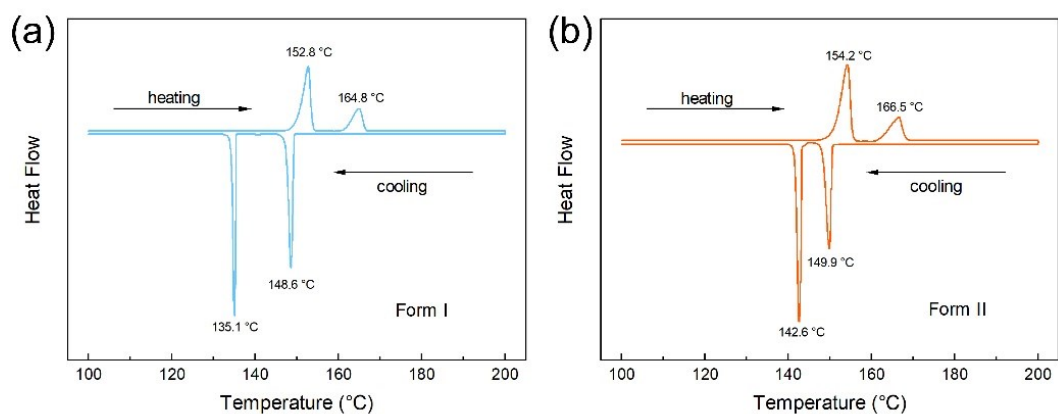
2.5 Thermal and kinetic properties

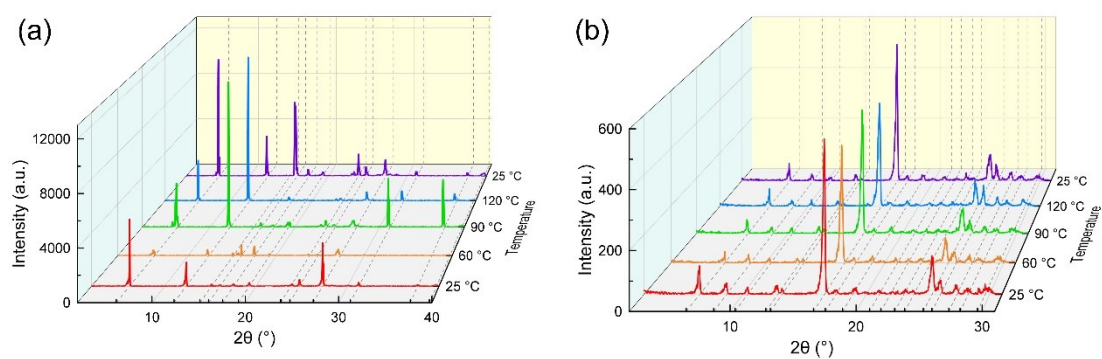**Fig. S10.** The DSC curves of *trans-*AzC$_2$ (a) Form I and (b) Form II crystals.

Fig. S11. Variable-temperature PXRD patterns of (a) Form I and (b) Form II crystals over the temperature range of 25-120 °C on heating and then cooling.
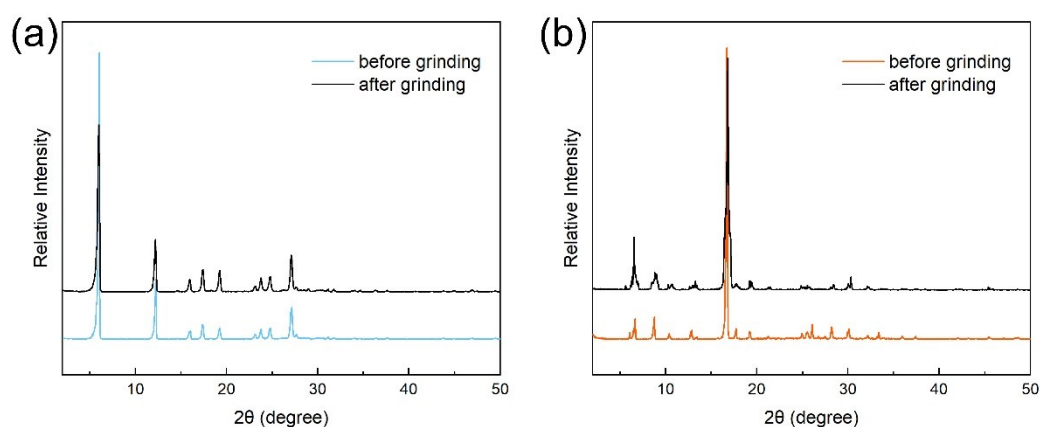

Fig. S12. PXRD patterns of (a) Form I and (b) Form II before and after grinding for 10 min.

3. Photomechanical Deformation

3.1 Reversible photoisomerization properties

Photoisomerization of the AzC_2 compound in the free state ($CDCl_3$ solution) was investigated by ^1H NMR spectra (Fig. S13). The ***trans/cis***-ratio calculation was based on comparing the average peak areas of AzC_2 protons (1-12), which include protons (1-6) from ***trans***-AzC_2 and protons (7-12) from ***cis***-AzC_2. Before UV irradiation, the ***trans***- percentage of the AzC_2 solution was over 99 %. After 365 nm UV irradiation (150 mW/cm^2) for 10 min to ensure achieved photostationary states, 81 % of the ***trans***- isomers isomerized into ***cis***- isomers. With subsequent stopping illumination for 6 h, ***cis***- isomers switched back to ***trans***- isomers to reach a ***trans***- percentage of 77 %. And after stopping illumination for 1 day, the ***trans***- percentage of the AzC_2 solution was recovered over 99 %.
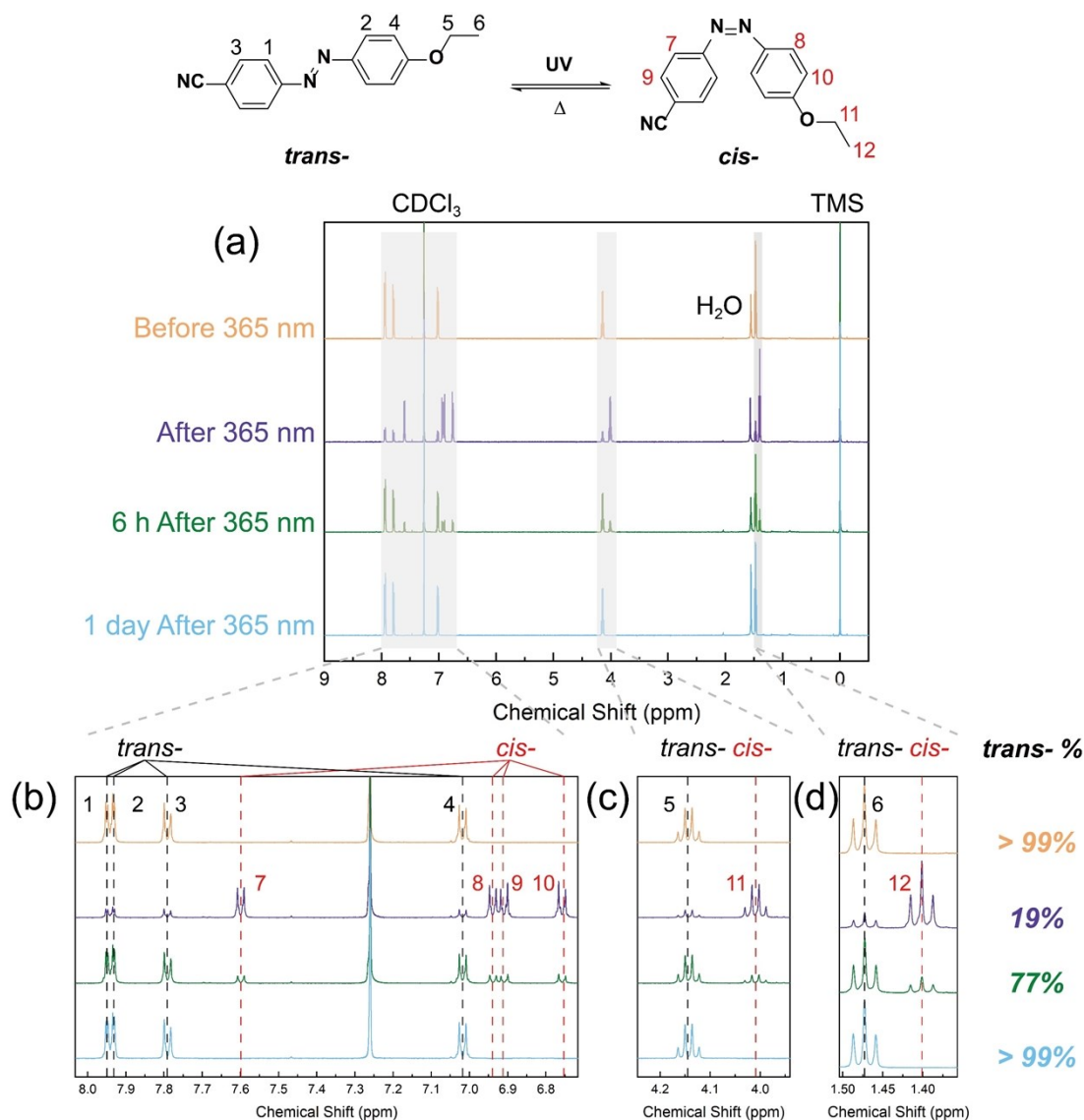

Fig. S13. ^1H NMR spectra of AzC_2 compound in $CDCl_3$ solution showing reversible photoisomerization upon irradiation with UV light and thermal relaxation.

The reversible photoisomerization behavior of the obtained two polymorphic microcrystals were characterized by Raman spectroscopy respectively. Generally, the *trans-*isomer has strong stretching vibrations since its molecular structure is planar, while the *cis-*isomer exhibits obvious torsional vibration since *cis-*molecules have a dihedral angle.[2, 3] These differences can be used to monitor the compositional changes between isomers.

The Raman spectra of Form I and Form II microcrystals have distinctive features in the range of 1200 ~ 1100 cm^{-1} due to significantly different packing patterns (Fig. S14 a). Upon UV irradiation (365 nm, 150 mW/cm^2), the intensity of peaks representing vibrations of *trans-* isomer in Form I decreased, whereas several new vibrations peaks appeared (Fig. S14 b), such as the peaks at 1500 and 1314 cm^{-1} (N=N stretch), 1302 cm^{-1} (NCC deformation), 926 and 791 cm^{-1} (C-N=N-C torsion). Moreover, the C-N stretch represented by peaks at 1195 and 1185 cm^{-1} combined into 1195 cm^{-1}. This could be explained by the appearance of the *cis-*isomer, which is caused by the transformation of planar molecules into steric molecules. After stopping UV irradiation for 10 min, the Raman spectrum of Form I microcrystals almost recovered its initial shape. The Raman spectra of Form II microcrystals showed similar changes (Fig. S14 c). Upon the same UV irradiated condition, the intensity of peaks representing vibrations of *trans-* isomer in Form II decreased, while some new vibrations peaks appeared, such as the peaks at 1541 and 1321 cm^{-1} (N=N stretch), 1304 cm^{-1} (NCC deformation), 1224 cm^{-1} (CCH deformation within the phenyl rings), 919 and 839 cm^{-1} (C-N=N-C torsion). This could also be explained by the photoisomerization from *trans-* to *cis-* isomers. After stopping UV irradiation for 10 min, the Raman spectrum of Form II microcrystals almost recovered its initial shape. The band assignments of *trans-* and *cis-* isomer in both polymorphisms were summarized in Table S2.

By comparing Fig. S14 b and c, we noticed that the Raman peaks representing vibrations of *trans-* isomer in two polymorphic microcrystals still existed upon UV irradiation, indicating only partial AzC_2 molecules underwent photoisomerization in both polymorphic microcrystals, and the photoisomerization is reversible. In addition, it could be noticed that the Raman spectrum of Form II changed more significantly under the same UV irradiation, which can qualitatively indicate that the photoisomerization ability of Form II is stronger than Form I.
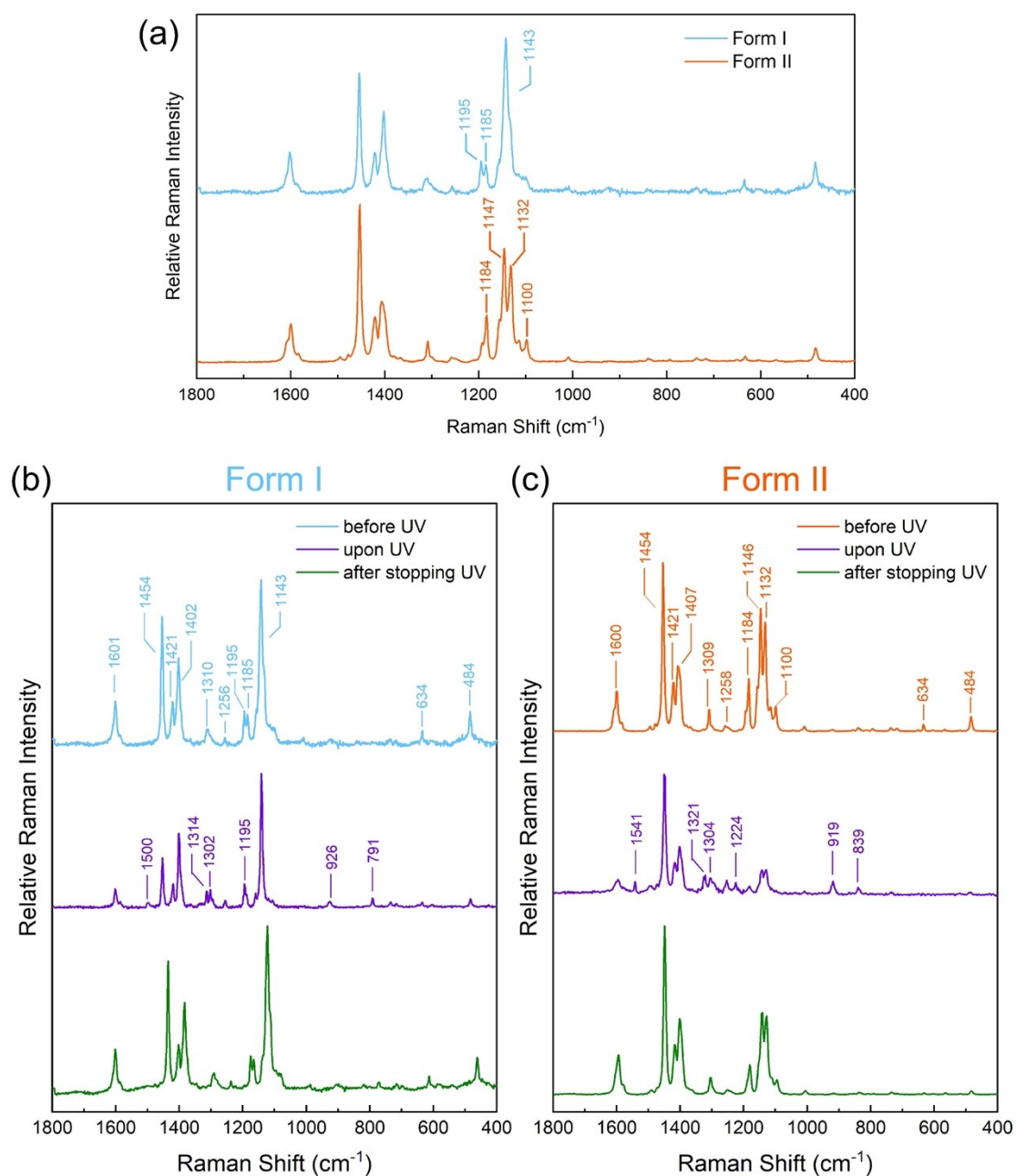
Fig. S14. (a) Comparison of Raman spectra of Form I and Form II microcrystals. Raman spectral changes of (b) Form I and (c) Form II microcrystals.

Table S2. Summary of Raman Shift for type of *trans-* and *cis-* isomer vibration in Form I and Form II.

Vibration [a]	Raman Shift (cm^{-1})			
	Form I		Form II	
	trans-	*cis-*	*trans-*	*cis-*
v (NN)	1601		1600	
	1454	1500	1454	1541
	1421	1314	1421	1321
	1402		1407	

δ (NCC)	1310	1302	1309	1304
δ (CCH) [b]	1256	1256	1258	1224
v (CN)	1195 1185	1195	1184	
δ (CNN)	1143	1143	1146 1132 1100	1146 1132
τ (CNNC)	-	926 791	-	919 839
δ (CCC) [b]	634	634	634	634
δ (COC)	484	484	484	484

[a] v = stretch, δ = deformation and τ = torsion.
[b] δ (CCH) and δ (CCC) is the motion within the phenyl rings.

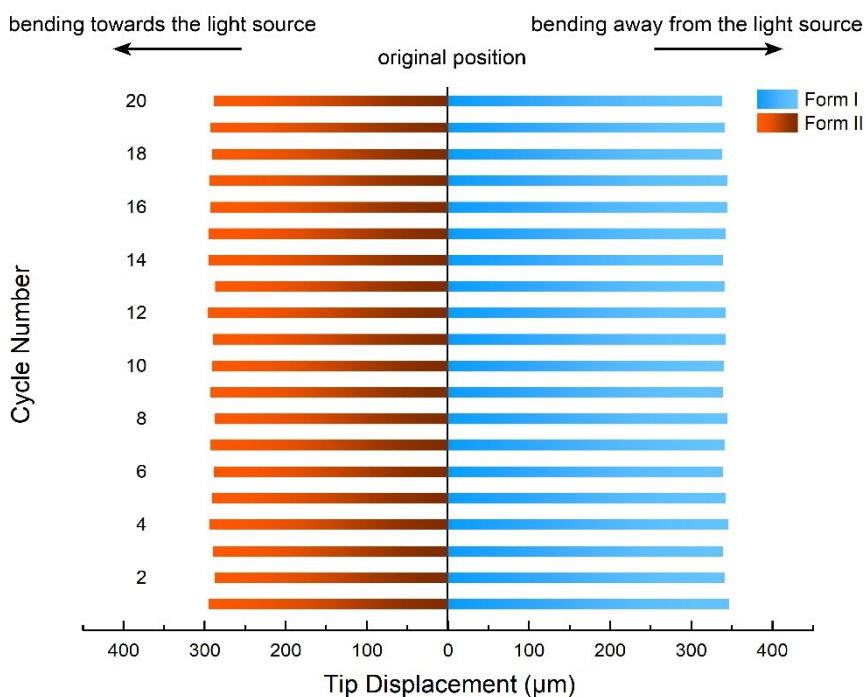## 3.2 Repeatability of photoinduced deformation behaviors

Fig. S15. The repeatability of the bending motion of the two polymorphs can be observed over 20 cycles.

3.3 Photothermal effect

The thermal effect of two polymorphic microcrystals under UV irradiation were measured by one infrared thermometer. UV light (150 mW/cm^2) irradiated from the top down, and the distance between the UV source and the microcrystals was about 5 cm. Due to limitation of resolution of the camera, cluster of microcrystals was used instead of one single microcrystal. As shown in Fig. S16, the highest temperature of Form I

microcrystals under UV irradiation was 25 °C in 5 s, and that of Form II microcrystals under UV irradiation was 28 °C in 5 s. Photoirradiation did not cause significant temperature increase in both polymorphic microcrystals, indicating that there is no obvious photothermal effect, which excluded the possibility of thermal effects induced photomechanical deformations.
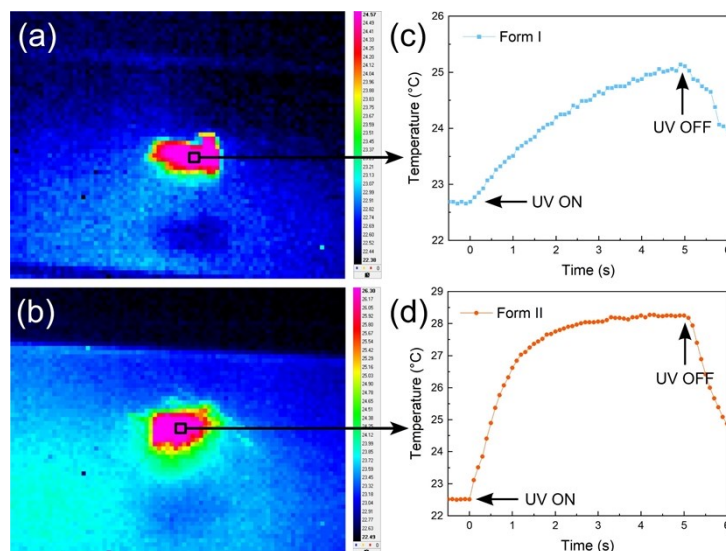

Fig. S16. Infrared images of a cluster of (a) Form I and (c) Form II microcrystals under UV irradiation (150 mW/cm2). And (b, d) their temperature change as a function of photoirradiation time.

3.4 Effects of irradiated time and directions on the photomechanical deformations

As shown in Fig. S17 and Movie S3, the plate-like microcrystal of Form I (size: 1358 μm ×317 μm × 8 μm) showed mono-directional motion under the UV light (365 nm, 150 mW/cm^2). When the (020) surface was irradiated from the left, the microcrystal quickly bent away from the light source to reach a maximum tip displacement of 138 μm within 0.2 s (Fig. S17b). Photoirradiation for longer durations (15 s) did not lead to any more significant deformation to the Form I microcrystal (Fig. S17c). Subsequent removal of the illumination resulted in immediate returning back to

its initial shape (Fig. S17d). When the $(0\bar{2}0)$ surface was irradiated from the right, the

microcrystal also quickly bent away from the light source to reach a maximum tip displacement of 54 μm within 0.2 s (Fig. S17e). Longer irradiated durations (15 s) did not lead to any more significant deformation either (Fig. S17f). After the irradiation was terminated, Form I microcrystal instantly regained its original straight shape (Fig. S17g).
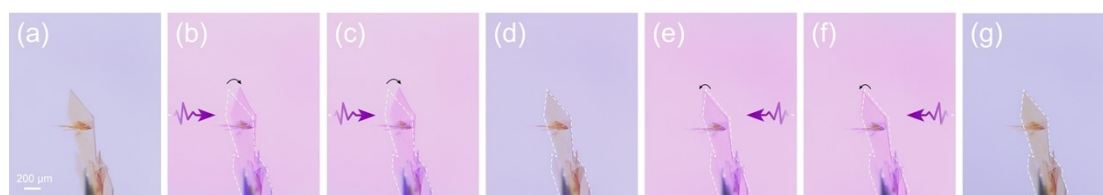
Fig. S17. Effects of irradiated time and irradiated directions on the photomechanical deformations of the plate-like microcrystal of Form I: (a) before irradiation, upon photoirradiation on the (020) surface from the left side for (b) 0.2 s and (c) 15 s, then (d) stopping the illumination. Next, upon photoirradiation on the $(0\bar{2}0)$ surface from the right side for (e) 0.2 s and (f) 15 s, and (g) subsequent stopping illumination.

As shown in Fig. S18 and Movie S4, the needle-like microcrystal of Form II (size: 2078 μm × 36 μm × 32 μm) also exhibited mono-directional motion under the UV irradiation (365 nm, 150 mW/cm^2). When the (012) surface was irradiated from the left, the microcrystal bent towards the light source to reach a maximum tip displacement of 207 μm within 1 s (Fig. S18b). Photoirradiation for longer durations (15 s) did not lead to any more significant deformation to the Form II microcrystal (Fig. S18c). Subsequent removal of the illumination resulted in immediate returning back to its initial shape (Fig. S18d). When the $(0\bar{1}2)$ surface was irradiated from the right, the microcrystal also bent towards the light source to reach a maximum tip displacement of 232 μm within 1 s (Fig. S18e). Longer irradiated durations (15 s) did not lead to any more significant deformation either (Fig. S18f). After the irradiation was terminated, Form II microcrystal instantly regained its original straight shape (Fig. S18g).
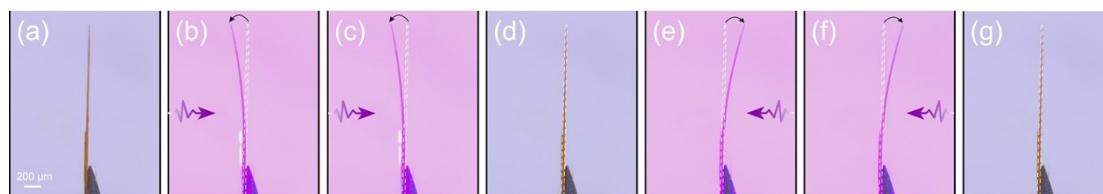

Fig. S18 Effects of irradiated time and irradiated directions on the photomechanical deformations of the needle-like microcrystal of Form II: (a) before irradiation, upon photoirradiation on the (012) surface from the left side for (b) 1 s and (c) 15 s, then (d) stopping the illumination. Next, upon photoirradiation on the $(0\bar{1}2)$ surface from the right side for (e) 1 s and (f) 15 s, and (g) subsequent stopping illumination.

3.5 Summary of the PXRD parametric variations of the crystal surfaces

Bragg's Law
$2d\sin\theta = n\lambda, n = 1,2...\#(1)$
where d is interplanar distance from lattice planes, θ is the glancing angle, n is a positive integer and λ is the wavelength of the incident wave.

Table S3. Summary of the PXRD parametric variations of the crystal faces.

surface	2θ (°)	d (Å)	Height	Area	FWHM

Form I	(020)	before	5.900	14.9674	14756	101523	0.117
		UV	6.119	14.4316	9236	93772	0.173
	(040)	before	12.099	7.3093	13460	85740	0.108
		UV	12.319	7.1792	8780	74054	0.143
Form II	(012)	before	16.401	5.4002	1661	7552	0.077
		UV	16.281	5.4399	652	5742	0.150

3.6 Theoretical calculation

The molecular geometry of *cis-*AzC$_2$ was optimized by Gaussian software using the B3LYP functional with the 6-31g(d) basis set. For optimization, constrain of the C-N=N-C torsion angles obtained from the crystal structure of cis-azobenzene was applied,[4] which is 53 ° for compound *cis-*AzC$_2$. Molecules of *trans-*AzC$_2$ in two polymorphs from crystal structures and optimized molecular structure of *cis-*AzC$_2$ are shown in Fig. S19.

In Form I, the length and width of *trans-*AzC$_2$ on (020) face are 5.261 Å and 9.113 Å and the thickness perpendicular to (020) face is 12.854 Å. Those of *cis-*AzC$_2$ are 6.853, 8.290 and 8.184 Å, respectively. In Form II, the length and width of *trans-*AzC$_2$ on (012) face are 11.202 Å and 11.300 Å and the thickness perpendicular to (012) face is 4.866 Å. Those of *cis-*AzC$_2$ are 8.582, 8.543 and 5.369 Å, respectively.
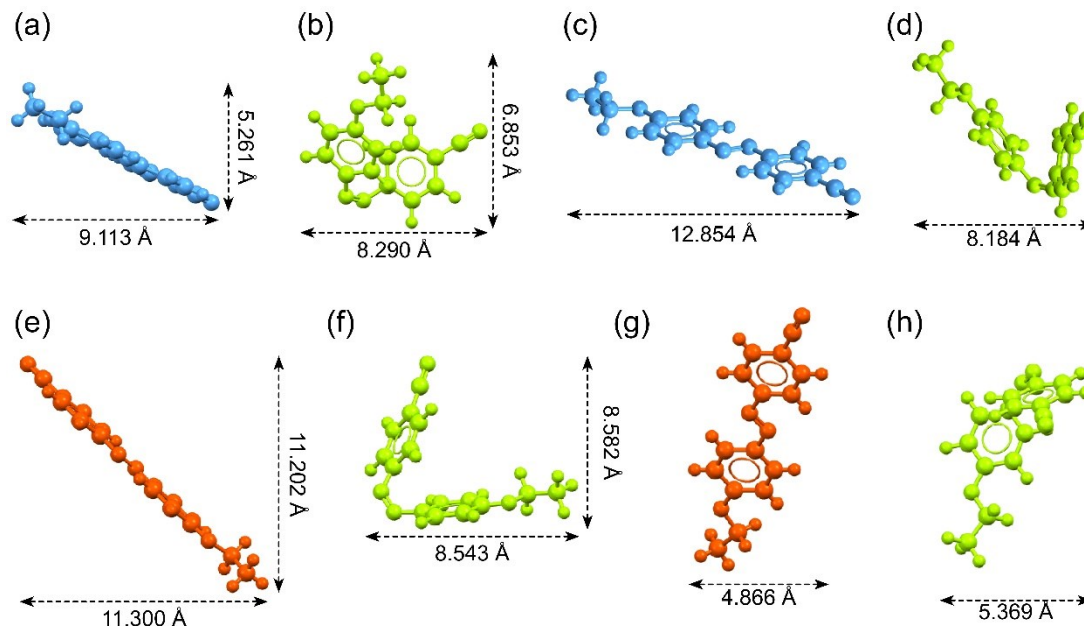

Fig. S19. The conformational size diagrams of *trans-*AzC$_2$ from Form I (blue) and the optimized molecular structure of *cis-*AzC$_2$ (green) on the (020) surface (a, b) and perpendicular to (020) surface (c, d). The conformational size diagrams of *trans-*AzC$_2$ from Form II (red) and the optimized molecular structure of *cis-*AzC$_2$ (green) on the (012) surface (e, f) and perpendicular to (012) surface (g, h).

4. Mechanical Behaviors

4.1 Nanoindentation test

Samples were adhered to metal sample disks with double-sided tape. The experiments were performed on (020) surface of Form I and (012) surface of Form II. In the loading phase, we performed the crystal to a maximum depth of 4000 nm within 10 s. h = 4000 nm was held for 1 s in the holding phase. In the unloading phase, the crystal was unloaded within 10 s.

Table S4. Summary of the elastic modulus and hardness of two polymorphs.

	Form I (020) surface				Form II (012) surface			
	Crystal 1	Crystal 2	Crystal 3	AVERAGE	Crystal 1	Crystal 2	Crystal 3	AVERAGE
Er (MPa)	181.503	189.739	226.236	199.159	5.131	7.419	3.698	5.416
H (MPa)	19.011	21.591	6.517	15.706	1.661	2.222	1.343	1.742

4.2 Dynamic mechanical analysis (DMA) tests

The samples were clamped by tension-film mode and double-sided tape was placed between grip and sample to minimize slippage during testing. 1 Hz was set as the frequency.
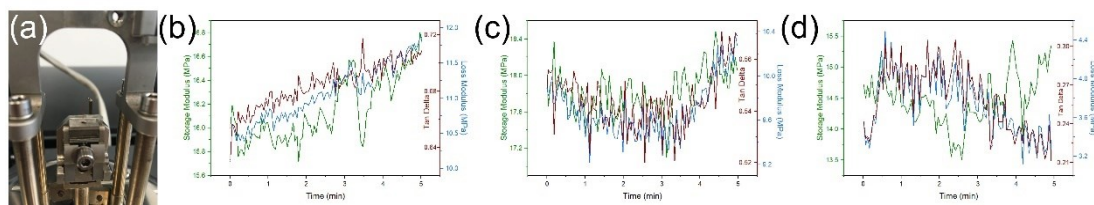

Fig. S20. (a) Photograph representing an acicular Form II crystal in the actual DMA testing system. (b-d) DMA-measured storage modulus, loss modulus, and tan delta of three individual acicular Form II crystal.

Table S5. Summary of the storage modulus, loss modulus and tan delta of three individual acicular Form II crystal.

Form II	Storage Modulus (MPa)	Loss Modulus (MPa)	Tan Delta
Crystal 1	16.159	11.070	0.685
Crystal 2	17.813	9.694	0.544
Crystal 3	14.479	3.745	0.259

4.3 Energy Frameworks

CrystalExplorer 17[5] was employed to calculate and visualize intermolecular

interaction energies based on Gaussian B3LYP/6-31G(d,p) molecular wavefunctions. Atoms were generated within 25 Å. The tube size in the energy frameworks of both two polymorphs is 100, and the cut-off energy value is 5 kJ·mol^{-1}. The total energies of interaction between molecules include four components: electrostatic, polarization, dispersion and exchange-repulsion:

$$E_{tot} = k_{ele}E_{ele} + k_{pol}E_{pol} + k_{dis}E_{dis} + k_{rep}E_{rep} \#(2)$$

where k refers to scale factor for benchmarked energy models.[6]
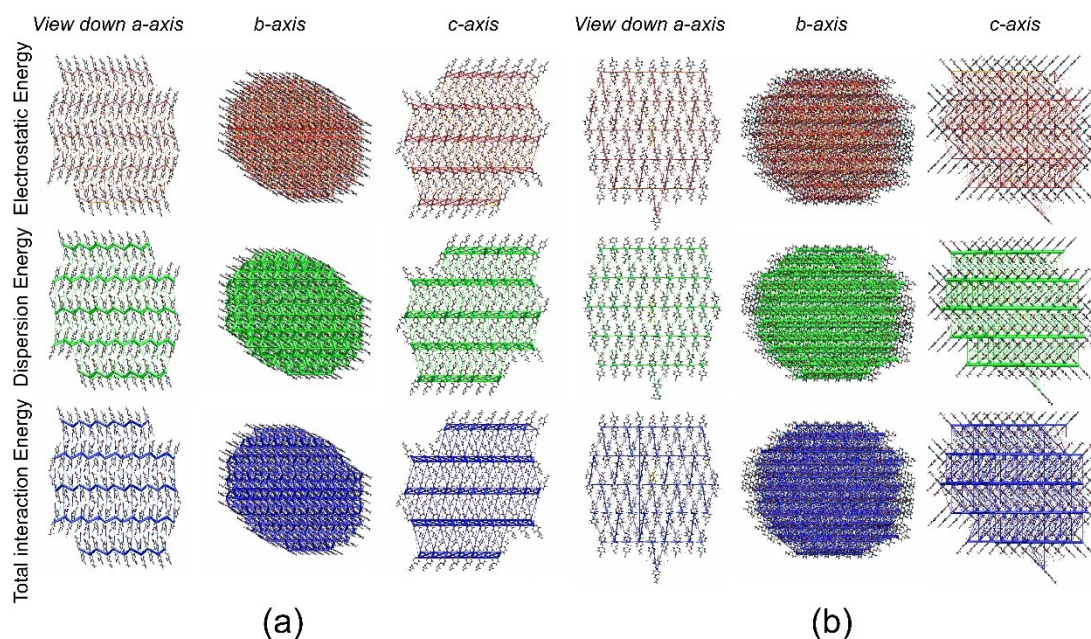

Fig. S21. Energy frameworks corresponding to the electrostatic, dispersion and total interaction energy components in (a) Form I and (b) Form II, respectively.

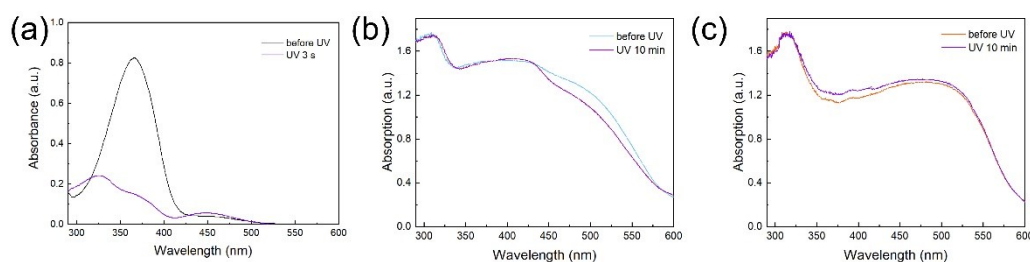## 5. Photoluminescent Behaviors

5.1 Absorption spectra

Fig. S22. (a) UV-vis absorption spectral change of trans-AzC2 (0.05 mM) in THF solution upon 3 s irradiation of UV light (80 mW/cm^2). UV-Vis diffuse reflection spectral changes upon 10 min UV irradiation (150 mW/cm^2) of (b) Form I and (c) Form II.
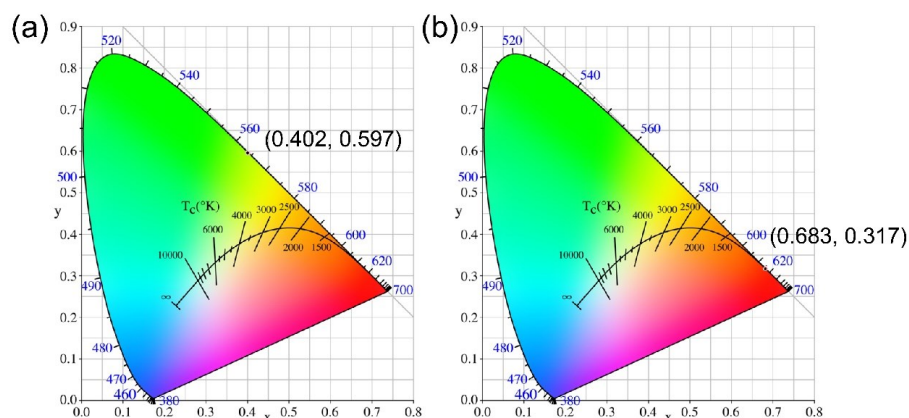
5.2 CIE 1931 chromaticity diagram

Fig. S23. CIE 1931 coordinates of (a) Form I and (b) Form II.

5.3 Crystal voids

Although isomerization has been suppressed by dense packing, AzC_2 molecules in crystalline state can still absorb energy and undergo very small geometric deformations upon UV irradiation. Sufficient free spaces are essential for the conformational change of molecules. The crystal voids (empty regions of a crystal structure) were calculated and visualized by CrystalExplorer 17 under the conditions of isovalue 0.002 e au^{-3}.

It can be seen from the void maps results shown in Fig. S24 that the void spaces of Form II are uniformly distributed around AzC_2 molecules. In contrast, the void spaces of Form I are mainly distributed at the head and tail of AzC_2 molecules, while fewer void spaces in other two orthogonal directions greatly limit the conformational changes of the molecules. Therefore, AzC_2 molecules in Form II have more possibility to have relatively larger geometric deformation under the same irradiation. This non-radiative process would consume much excitation energy and weaken luminescence.
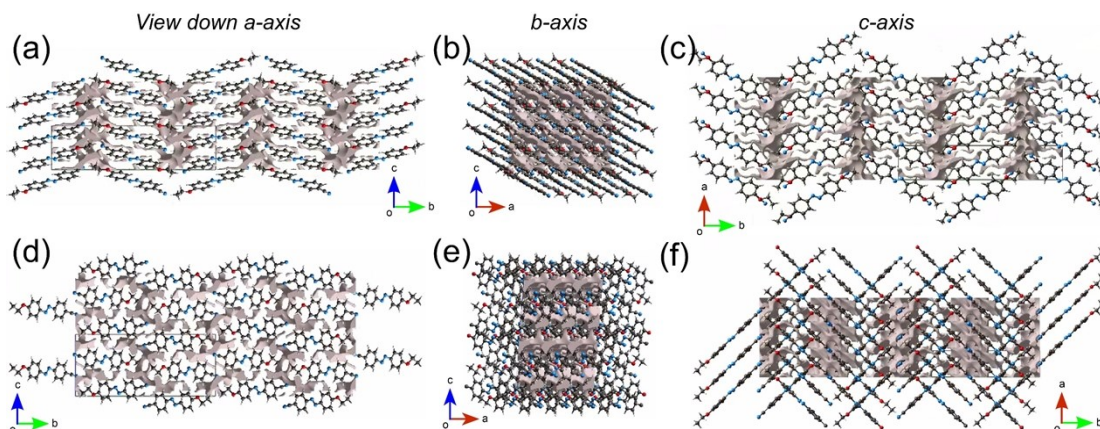
Fig. S24. Void maps in the crystal structures of (a-c) Form I and (d-f) Form II.

5.4 Photoluminescent spectra of two polymorphic microcrystals

The maximum emission wavelengths of the two polymorphic microcrystals which exhibit photomechanical deformation appear over 700 nm (Fig. S25a). Their relatively loose packings make isomerization less suppressed (Fig. S25b). In this case, more excitation energy is used for isomerization and less energy is used for luminescence, which results in a red shift of the maximum emission wavelength.
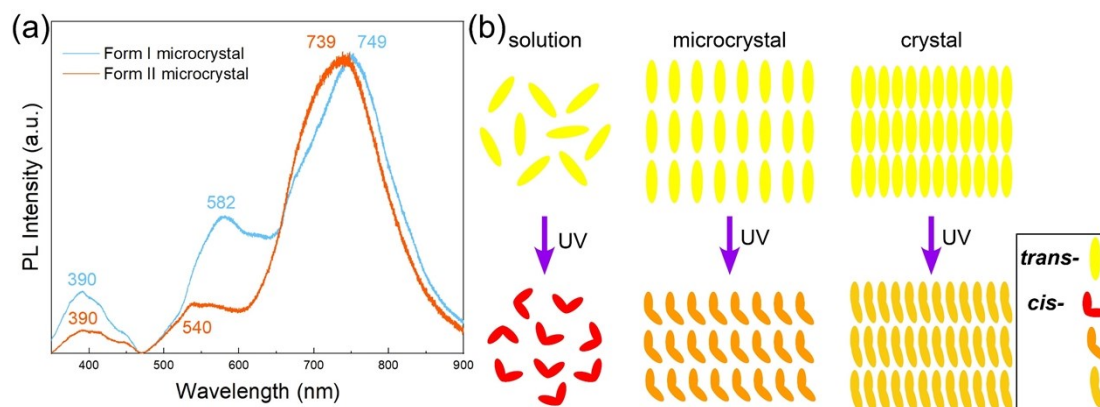

Fig. S25. (a) Photoluminescent spectra of two polymorphs microcrystals. (b) Schematic illustration of effect of molecular packing density on photoisomerization ability.

6. Supplementary movie legends

Movie S1. Photoinduced reversible bending motion of one plate-like Form I microcrystal bend away from the light source.

Movie S2. Photoinduced reversible bending motion of one needle-like Form II microcrystal bend towards to the light source.

Movie S3. Effects of irradiated time and directions on the photomechanical deformations of one plate-like Form I microcrystal.

Movie S4. Effects of irradiated time and directions on the photomechanical deformations of one needle-like Form II microcrystal.

Movie S5. Brittle breaking of Form I crystal.

Movie S6. Elastic bending of Form II crystal from the (012) face.

Movie S7. Elastic bending of Form II crystal from the (020) face.

Movie S8. Plastic deformation of the much thinner Form II crystal.

7. References

(1)   Hao, Y.; Huang, S.; Guo, Y.; Zhou, L.; Hao, H.; Barrett, C. J.; Yu, H., Photoinduced multi-directional deformation of azobenzene molecular crystals. *Journal of Materials Chemistry C* **2019,** 7, (3), 503-508.

(2)   Stuart, C. M.; Frontiera, R. R.; Mathies, R. A., Excited-State Structure and Dynamics of cis- and trans-Azobenzene from Resonance Raman Intensity Analysis. *The Journal of Physical Chemistry A* **2007,** 111, (48), 12072-12080.

(3)   Larkin, P. J., Infrared and Raman Spectroscopy; Principles and Spectral Interpretation. *Elsevier* **2011**.

(4)   Mostad, A.; Rømming, C., A Refinement of the Crystal Structure of cis-Azobenzene. *Acta Chem. Scand* **1971,** 25, 3561 –3568.

(5)   M. J. Turner; J. J. McKinnon; S. K. Wolff; D. J. Grimwood; P. R.Spackman; Jayatilaka, D.; Spackman, M. A., CrystalExplorer17. *University of Western Australia* **2017**.

(6)   Turner, M. J.; Thomas, S. P.; Shi, M. W.; Jayatilaka, D.; Spackman, M. A., Energy frameworks: insights into interaction anisotropy and the mechanical properties of molecular crystals. *Chem Commun (Camb)* **2015,** 51, (18), 3735-8.